J. Fluid Mech. (1989), *vol.* 206, *pp.* 405–432
Printed in Great Britain

Stability of Long's vortex at large flow force

By M. R. FOSTER[1] AND F. T. SMITH[2]

[1] Department of Aeronautical and Astronautical Engineering, The Ohio State University, 203 Neil Avenue Mall, Columbus, OH 43210-1276, USA

[2] Department of Mathematics, University College London, Gower Street, London WC1E 6BT, UK

(Received 18 February 1988 and in revised form 21 February 1989)

Long's self-similar vortex is known to have two solutions for each supercritical value of the flow force. Each of those solutions is shown here to have a double structure if the flow force is large. We then investigate the inertial instabilities of one of those large-flow-force limit solutions, and find them to be related to the instabilities of the Bickley jet in one régime. However, the swirl in the vortex becomes important for long waves, very strongly modifying the sinuous and varicose Bickley modes. We find in particular that the asymptotic results obtained agree well with our numerical solutions for the sinuous mode, but not for the varicose mode, the difficulty in the latter case being apparently due to mode jumping. The asymptotics show a varicose long-wave neutral mode for positive azimuthal wavenumber, and two such modes for negative wavenumbers. The upper neutral sinuous mode occurs at much larger wavenumber than in the Bickley case, and its structure is also presented. The study overall is aimed at providing a basis for the investigation of strongly nonlinear effects.

1. Introduction

Vortex breakdown, multiple vortex structures and other intriguing phenomena are common to the motion of atmospheric vortices as well as in leading-edge, wing-tip, and other vortices in airfoil flight, and also in pipe flows and other confined swirling flows. Many studies of such phenomena have been presented, among them Howard & Gupta (1962), Pedley (1968, 1969), Lessen & Singh (1973), Lessen, Desphande & Hadji-Ohanes (1973), Lessen, Singh & Paillet (1974) and Burggraf & Foster (1977*b*). In the atmospheric setting, both Snow (1978) and Staley & Gall (1979) have attempted to model instabilities in tornado vortices.

Most of the studies, including Staley & Gall (1979), Snow (1978), and Lessen *et al.* (1973), have dealt with broken-line profiles, or even vortices without any axial shear whatever. Exceptions are Lessen *et al.* (1974), and a series of papers by Stewartson (1982), Maslowe & Stewartson (1982), Leibovich & Stewartson (1983), Stewartson & Capell (1985), Duck (1986), and Stewartson & Leibovich (1987). Also, Duck & Foster (1980) and Foster & Duck (1982) explore instabilities of full three-dimensional vortices.

The sequence of papers above, beginning with Stewartson (1982), utilizes asymptotic methods to explore the instability of certain profiles for large azimuthal wavenumber. Leibovich & Stewartson (1983) and independently Duck (1986) found thereby a hitherto-unknown sufficient condition for instability of such swirling flows. These investigators focused on the Batchelor (1964) trailing-vortex solution, although there turns out to be much generality in the analysis.

The motivation for the present work comes from the fact that most previous theories have been for linear disturbances whereas the most significant of vortex phenomena, including vortex breakdown, would seem rather to be strongly nonlinear processes. There have been few if any fully nonlinear analysis attempted or reported in the literature, however, and so the current study is undertaken deliberately with a view to its extension subsequently to the fully nonlinear regime. That enlargement into the fully nonlinear regime, i.e. where the mean-flow profile is completely altered from its original state, appears to be more readily achievble from the basis established in this work owing to its interactive flow-structural nature, an aspect discussed later in the paper. Here, therefore, we extend analytically, to large values of flow force, the work of Foster & Duck (1982) on the instability modes of the self-similar vortex family due to Long (1961) in which the swirl and axial velocity variations with radius are suggestive of what one might find in a tornado vortex:† cf. Hoecker (1960) and Burggraf & Foster (1977*b*) for more discussion of this point. The vortex, then, is an exact solution of the Navier–Stokes equations at large values of the effective Reynolds number, Γ/ν, where Γ is the vortex circulation and ν is the kinematic viscosity of the fluid. Although the details of the solution are summarized in §3 below, we note at this point that the swirl and axial velocity components are functions of the conical variable $\Gamma r/2\sqrt{2\pi\nu z}$, with (r, z) being the radial and axial coordinates. These vortex solutions may be characterized by the value of the 'flow force',

$$J = \frac{\rho\Gamma^2}{4\pi^2}M = 2\int_0^\infty (p - p_\infty + \tfrac{1}{2}\rho w^2)\, r\, \mathrm{d}r, \tag{1.1}$$

which represents in effect the relative strength of the axial flow in the vortex. Two solutions exist for each value of M exceeding $M_c = 3.75$ and none for $M < M_c$, as indicated by figure 1. Figure 2 shows both sets of axial velocity and swirl velocity profiles for this vortex for a value of M of 4.00. All of the vortices of this family are unstable to small disturbances for sufficiently large negative values of the azimuthal wavenumber, n, of the disturbance, by application of the Leibovich–Stewartson criterion. Foster & Duck (1982) found unstable modes numerically for negative but finite n, but were unable to compute any modes for positive n, a feature also true for the Batchelor vortex, as noted in Duck & Foster (1980): see later comments in this section.

In this paper we describe first the asymptotic basic-flow profiles at large values of the flow force M for both Type I and Type II profiles (§3), and then study, in §§4 and 5, the two families ('sinuous' and 'varicose' as defined subsequently) of instability modes that arise for finite $|n|$ for the Type II vortex. Comparisons with computational results are also presented.

We find that the basic Type II vortex at large M consists of a large cylinder of radius M containing fluid that is slowly flowing downward and has virtually no azimuthal motion. At the radius M the swirl rises rapidly to that for a potential vortex over a relatively narrow $O(1)$ zone in which there is an intense upward ring jet (with a sech^2 profile). Exterior to this radius, the azimuthal motion is that of a potential vortex, and the axial motion is weak, decaying at large radius. It is not surprising, then, that for axial wavelengths of the order of this jet width the stability

† There is good evidence that there is an off-axis velocity peak in waterspouts, which are dynamically nearly identical to tornadoes (see Church & Ehresman 1971, and Golden 1973). The Type II Long's vortex profile examined in this paper has exactly that form! So, in fact, the profile chosen here is sensible in the light of these observations.

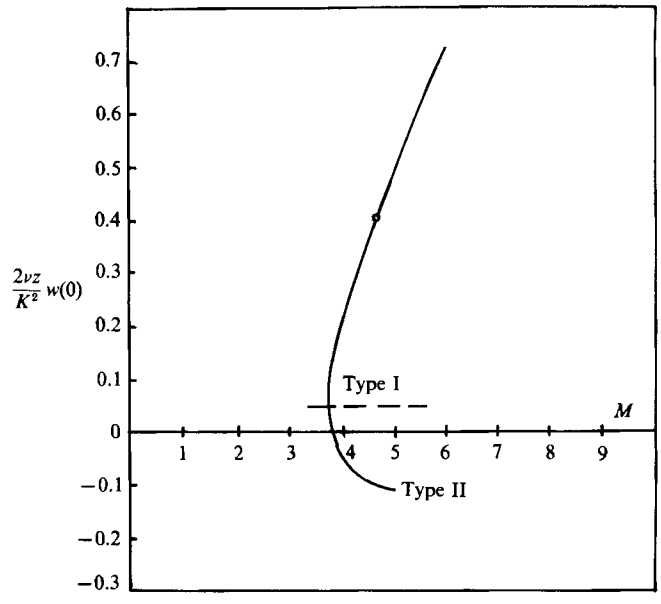

FIGURE 1. The vertical velocity on the axis for Long's vortex *vs.* flow force, M, showing the Type I and Type II families. The results are established in Foster & Duck (1982). All vortices below $M = 4.71$ (○) are of defect type, i.e. the axial velocity maximum is off-axis.

character of the flow is essentially that of the Bickley jet (Drazin & Reid 1981) and is almost two-dimensional. However, as the waves become longer, the first distinctive length being of order M, the double structure of the basic vortex becomes important, as does the azimuthal convection of the velocity perturbations, so that the angular momentum in the vortex comes into play. This changes the instability modes away from the sinuous and varicose two-dimensional Bickley modes into three-dimensional ones, which are governed by an interactive structure in the sense that the ring-jet-region's influence is counterbalanced by that of the weaker vortex flow outside the ring jet.

We find further that for M large there is no computational or analytic barrier to obtaining unstable modes for n negative *or* for n positive in the present flow, whereas Duck (1986) by contrast found no evidence for modes at large positive n in the case of the Batchelor vortex: see also our earlier comments. The present evidence suggests that, beyond some positive value of M, positive-n modes do arise. A similar conclusion applies to the other, Type I, vortex flow since it approaches the Squire-jet form for M large, thus yielding instabilities for $n = +1$ as well as for $n = -1$.

Further comments, including mention of the nonlinear regime, are presented in §6.

Finally, although the Bickely-jet instabilities exist up to a finite wavenumber, the cut-off wavenumber in the case of our vortex is substantially different owing to the swirl effects The analysis leading to that cut-off value for the sinuous mode is presented in the Appendix.

To be complete, it should be noted that an actual tornado has complexities not incorporated in the analysis of this paper. Certainly, the connections of the tornado vortex to the 'collar cloud' above it and in general to the parent thunderstorm are important, particularly with regard to initiation of the tornado. However, it may be that, once the tornado vortex is formed, many of the complexities of the thunderstorm environment, like release of latent heat for example, are less important

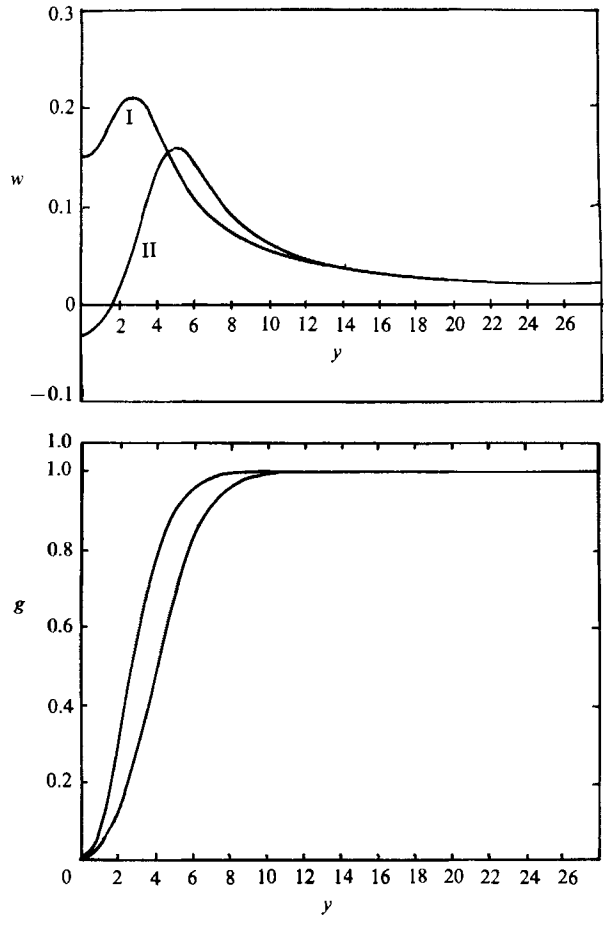

FIGURE 2. Dimensionless axial velocity and angular momentum computed for Long's vortex, Types I and II, for $M = 4.0$.

to the ongoing dynamics in the vortex itself than factors like hydrodynamic instability, turbulence, vortex breakdown, and other phenomena described by an homogeneous, incompressible model. On the other hand, density stratification in the ambient – and consequent buoyancy force – is likely to be significant to a very tall 'fully developed' vortex, say beneath a high cloud base. Pressure variations cause negligible density variations, however, since even the most generous estimates of velocities in tornadoes would put the square of the Mach number at $\frac{1}{4}$. Further, tornado morphology is varied; many – apparently including some of the most damaging – are rather short and wide, whereas the vortex studied here is long and slender. So, with such caveats in mind, we proceeed.

2. The governing equations

As in Foster & Duck (1982), we investigate the inviscid stability of Long's vortex by writing

$$\boldsymbol{u} = \boldsymbol{u}_0(r) + \tilde{\boldsymbol{u}}(r)\, \mathrm{e}^{\mathrm{i}k(z-ct)+\mathrm{i}n\theta}, \tag{2.1a}$$

$$p = p_0(r) + \tilde{p}(r)\, \mathrm{e}^{\mathrm{i}k(z-ct)+\mathrm{i}n\theta}, \tag{2.1b}$$

and substituting into the Euler equations. Here $\boldsymbol{u}_0$ is the basic flow which is described further in the next section and $\tilde{\boldsymbol{u}}$ is the small perturbation. In the usual way, we neglect all but the linear terms controlling $\tilde{\boldsymbol{u}}$ and, also consistent with the 'parallel-flow approximation', the z-dependence of the basic flow, $\boldsymbol{u}_0$, can be ignored to leading order. (The latter step can be justified *a posterioroi* for the solutions that are found subsequently: see also the end of this section.) Under these assumptions, the resulting equations reduce to the following pair governing $\tilde{\boldsymbol{u}}(y), \tilde{p}(y)$, where we hereafter omit the tildas:

$$\frac{\mathrm{d}u}{\mathrm{d}y} = \left(\frac{n g_0' + k y^2 w_0'}{y^2 \phi} - \frac{1}{y}\right) u + \mathrm{i} \frac{n^2 + k^2 y^2}{y^2 \phi} p, \tag{2.2a}$$

$$\frac{\mathrm{d}p}{\mathrm{d}y} = \mathrm{i}\left(\frac{(g_0^2)'}{y^3 \phi} - \phi\right) u - \frac{2n g_0}{y^3 \phi} p, \tag{2.2b}$$

$$\phi = k(w_0 - c) + \frac{n g_0}{y^2}, \tag{2.2c}$$

with u being the radial velocity perturbation and p the pressure, and the prime denotes differentiation with respect to y, a non-dimensional radial variable, r/L. g_0 and w_0 are respectively dimensionless angular momentum and axial velocity of the basic vortex, made dimensionless with $K = \Gamma/2\pi$ and K/L respectively. These equations, as such, apply of course to any vortex under a parallel-flow assumption. In our case we consider Long's conical self-similar vortex, discussed briefly in §1 and described in detail in §3. If z_0 is the distance to the virtual origin of the cone, then L must be $\sqrt{2\nu z_0/K}$ (see §3). The boundary conditions on (u, p) are

$$p(0) = \delta_{|n|,0}, \tag{2.3a}$$

$$u(0) = \delta_{|n|,1}, \tag{2.3b}$$

at the vortex centre, and the disturbances must decay for $y \to \infty$. Burggraf & Foster (1977*a*) noted that the appropriate condition to use at the vortex edge, in order to suppress the growing solution for $y \to \infty$ in the computations, is $p + \mathrm{i}cu = 0$. (There is some discussion of the rationale for this choice in §6.) In the analysis presented here we are able to use simply

$$p \to 0, \quad u \to 0 \quad \text{for} \quad y \to \infty. \tag{2.4}$$

It is these equations, (2.2)–(2.4), that we propose to solve to determine the complex wave speed $c = c_\mathrm{R} + \mathrm{i}c_\mathrm{I}$ for real wavenumber k (and azimuthal integers n) and hence obtain the instability properties for the vortex in question here. Analytical properties are discussed in §§4 and 5 and are compared there and in §6 with computational results.

The neglect of the viscous terms in the formulation means that the wavelengths cannot be too short (specifically, $k, n \ll (\Gamma/\nu)^{\frac{1}{2}}$); the parallel-flow condition assumed above also restricts the results. The local 'thickness' of the vortex is based on the distance $\mathbf{z}_0$ from the cone apex, and is proportional to $\nu z_0/\Gamma$. A term like $\partial w_0/\partial z$ may then be neglected in (2.2) only if $kz_0 \gg 1$. Since in this work k is assumed as small as M^{-2} in one case (see §4), the following restrictions,

$$|n| \ll (\Gamma/\nu)^{\frac{1}{2}}, \quad M \ll z_0^{\frac{1}{2}}, \tag{2.5}$$

then hold for the analysis.

3. The asymptotic vortex solutions

The basic flow itself is addressed now. The self-similar vortex solution found by Long (1961) has a stream function f, circulation and pressure that satisfy the following ordinary differential equations:

$$yf''-(1-f)f'-4y^3s=0, \tag{3.1}$$

$$yg''-(1-f)g'=0, \tag{3.2}$$

$$2y^3s'+g^2=0. \tag{3.3}$$

Here s is the pressure and the axial and swirl velocities are given by

$$w=\frac{K^2}{2\nu z}\frac{f'(y)}{y}. \tag{3.4}$$

$$v=\frac{K}{r}g(y), \tag{3.5}$$

where we recall that K denotes $\Gamma/2\pi$, with Γ being the circulation at the vortex edge, while (r,z) are radial and axial coordinates, ν is the kinematic viscosity of the fluid and y is the similarity variable $Kr/\sqrt{2\nu z}$. The boundary conditions are

$$f(0)=f'(0)=g(0)=0, \tag{3.6}$$

$$f'(\infty)=g(\infty)=1. \tag{3.7}$$

Long characterized the solutions to (3.1)–(3.7) in terms of a 'flow force', whose non-dimensional definition is, noting (1.1),

$$M=\pi\int_0^\infty((f')^2-g^2)\frac{dy}{y}, \tag{3.8}$$

and he observed that there are two solutions to the above family of nonlinear equations for M exceeding a critical value of $M_c=3.65$. (Actually, the critical value has been shown to be 3.75 in more accurate calculations by Burggraf & Foster 1977*b*.) Foster and Duck (1982) denoted these vortices as 'Type I' and 'Type II' based on the values of the axial velocity on the axis: see figure 1. Typical Type I and Type II profiles for axial and azimuthal velocity components are shown in figure 2, for $M=4$. We present in this section asymptotic solutions to (3.1)–(3.7) for large M, for both Type I and Type II vortices.

3.1. *Type I vortex*

The most substantial part of the axial motion in this case is a jet confined to a thin region around the axis $y=0$, with relative error $O(M^{-1})$. Thus we write $y=M^{-\frac{1}{2}}\eta$ and expand f, g, s as

$$\left.\begin{aligned} f&=F_0(\eta)+M^{-1}F_1(\eta)+\dots,\\ g&=G_0(\eta)+M^{-1}G_1(\eta)+\dots,\\ s&=MS_0(\eta)+S_1(\eta)+\dots, \end{aligned}\right\} \tag{3.9}$$

in which case the flow-force integral (3.8) reduces, to leading order, to

$$\int_0^\infty (F_0')^2\frac{d\eta}{\eta}=\frac{1}{\pi}. \tag{3.10}$$

Substitution of (3.9) into (3.1)–(3.3) then leads to the nonlinear governing equations

$$\left.\begin{aligned} \eta F_0'' - (1-F_0)F_0' &= 0, \\ \eta G_0'' - (1-F_0)G_0' &= 0, \\ 2\eta^3 S_0' + G^2 &= 0, \end{aligned}\right\} \tag{3.11}$$

whose solution is given by

$$F_0 = \frac{2k^2\eta^2}{1+\frac{1}{2}k^2\eta^2}, \quad G_0 = \tfrac{1}{4}F_0, \quad S_0 = \frac{\frac{1}{8}k^2}{1+\frac{1}{2}k^2\eta^2} \tag{3.12}$$

and the quantity k^2 is found from (3.10) to be $\frac{3}{16}\pi$. The solution (3.12) is exactly that for the round jet found by Squire (1951).

Construction of the solution for the next-order terms in the series (3.9) is technically difficult, and, without details, let it suffice to say that, for $\eta \to \infty$, $F_1 \sim \frac{1}{8}\eta^2$ whereas $F_0 \to 4$, and so the asymptotic expansion (3.9) is not uniformly valid for large η. We consider this feature next.

To examine the wider-scale structure, we write

$$\bar{f} = f(y), \quad g = 1 + M^{-1}\bar{g}(y), \quad s = (\tfrac{1}{4}y^2) + M^{-1}\bar{s}(y),$$

with y now of $O(1)$ as guided by (3.9), and then (3.1)–(3.3) reduce to the nonlinear form

$$y\bar{f}''' - (1-\bar{f})\bar{f}' = y, \tag{3.13a}$$

$$y\bar{g}'' - (1-\bar{f})\bar{g}' = 0, \tag{3.13b}$$

$$\bar{s}' - \bar{g}/y^3 = 0. \tag{3.13c}$$

A single integral of (3.13a) leads, however, to a Riccati equation whose solution is

$$\bar{f}(y) = y\frac{I_0(\frac{1}{2}y)}{I_1(\frac{1}{2}y)} \tag{3.14a}$$

where I_0 and I_1 are modified Bessel functions of the first kind (Abramowitz & Stegun 1965). The solution $\bar{f}$ can be shown to match to F_0 as $y \to 0$ and to satisfy the edge ($y \to \infty$) boundary conditions, as required. In addition, matching $\bar{g}$ to G, the swirl is given by

$$\bar{g}(y) = -\frac{4\pi}{3}\int_y^\infty \frac{\mathrm{d}\xi}{\xi(I_1(\frac{1}{2}\xi))^2}, \tag{3.14b}$$

from (3.13b). That completes the large-M structure of the Type I vortex.

3.2. *Type II vortex*

The previous numerical computations for this second vortex show the entire vortex growing in width, as measured by the position of the axial velocity peak, with increasing M. Hence, addressing the large-M behaviour, we write

$$f = y_0 F(Y), \quad g = G(Y), \quad s = y_0^{-2}S(Y),$$

where $Y = y/y_0$ is of order unity at first and y_0 is the parameter to be determined below that grows with increasing M. Substitution into (3.1)–(3.3) therefore gives the

leading-order terms in the associated asymptotic expansion satisfying the nonlinear system

$$\left.\begin{aligned} 2Y^3\frac{\mathrm{d}S_0}{\mathrm{d}Y}+G_0^2=0,\\ F_0\frac{\mathrm{d}G_0}{\mathrm{d}Y}=0,\\ F_0\frac{\mathrm{d}F_0}{\mathrm{d}Y}-4Y^3S_0=0. \end{aligned}\right\} \tag{3.15}$$

The required solutions here are found to be discontinuous across $Y=1$; specifically the solutions are

$$G_0=0,\quad F_0=\pm Y^2/\sqrt{2},\quad S_0=\tfrac{1}{4}\quad\text{in}\quad Y<1 \tag{3.16}$$

and

$$G_0=1,\quad F_0=(Y^2-\alpha^2)^{\frac{1}{2}},\quad S_0=1/(4Y^2)\quad\text{in}\quad Y>1, \tag{3.17}$$

where α is to be determined and the sign of the F_0 solution, (3.16), is not yet known either. Consequently a buffer layer or inner solution is induced near the cylindrical face $Y=1$.

The inner solution is obtained by writing $y=y_0+\xi, f=y_0\mathscr{F}(\xi)$, and $g=\mathscr{G}(\xi)$. The result of this to leading order is the set of equations,

$$\mathscr{F}''+\mathscr{F}\mathscr{F}'=0, \tag{3.18a}$$

$$\mathscr{G}''+\mathscr{F}\mathscr{G}'=0, \tag{3.18b}$$

obtained from (3.1) and (3.2). Any solution of (3.18 a) that will match to (3.16), (3.17) is easily seen to have the property that $\mathscr{F}\to c$ for $\xi\to\infty$ and $\mathscr{F}\to -c$ for $\xi\to-\infty$ for some constant, c. That result then resolves the ambiguity in the earlier-noted solution for F_0 in the outer flow, so that we have now

$$F_0=\begin{cases}-Y^2/\sqrt{2}, & Y<1,\\ (Y^2-\frac{1}{2})^{\frac{1}{2}}, & Y>1.\end{cases} \tag{3.19}$$

The inner solutions, when completed and matched with (3.16) and (3.17), are

$$\left.\begin{aligned} \mathscr{F}&=(1/\sqrt{2})\tanh(\xi_0),\\ \mathscr{G}(\xi)&=\tfrac{1}{2}[1+\tanh(\xi_0)]. \end{aligned}\right\} \tag{3.20}$$

Here, for convenience in what comes later, we use ξ_0 defined by

$$\xi_0=\tfrac{1}{2}(1+\xi/\sqrt{2}). \tag{3.21}$$

The location of the zero of ξ_0 in the solution comes about from the precise matching of the leading-order pressure. Further, the parameter y_0, introduced above, is readily found by substituting (3.20) into the flow-force definition (3.8) and is given by

$$y_0=(3\sqrt{2}/\pi)M.$$

So, in summary, the axial velocity in this Type II vortex has a very small downward drift inside the cylinder $y=y_0$, and a relatively high-speed jet-like region in the vicinity of $y=y_0$, given by

$$\mathscr{W}=\mathscr{F}'/\sqrt{2}=\frac{1}{4\sqrt{2}}\operatorname{sech}^2(\xi_0) \tag{3.22}$$

which is precisely the Bickley-jet solution. Across this same region, the swirl velocity rapidly adjusts from zero to the potential vortex solution. Outside of $y=y_0$ the basic

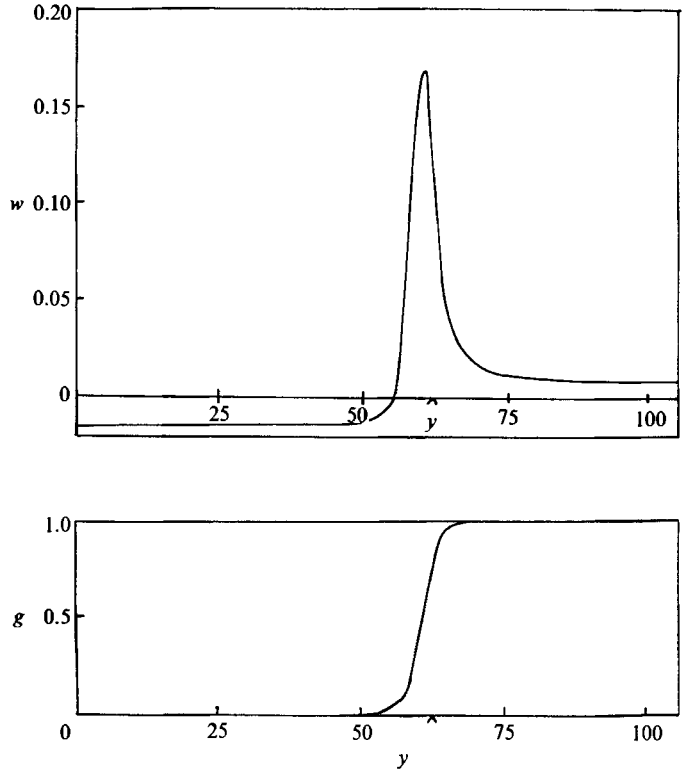

FIGURE 3. Dimensionless axial velocity and angular momentum computed for Long's vortex, Type II, for $M = 44.9$. The y_0-value is shown by a caret on the y-axis.

flow consists of much weaker axial velocity which decays algebraically. Figure 3 shows the computed velocities for $M = 44.9$, for which the above structure is evident.

We turn next to the instability features of the vortex motion.

4. Type II 'sinuous' inertial instability

We note from §3 that the Type II vortex solution for $M \to \infty$ mainly has the character of a ring jet of diameter $2y_0$, with its jet velocity profile given by the familiar sech^2 behaviour of the two-dimensional Bickley jet. In §2, the inertial instability problem was set. Note that if one inserts the Type II basic-flow solutions into (2.2), then with k of order unity the outer-flow eigenfunctions are trivial: see also below for other regimes. In the jet-like region, by contrast, where $y = y_0 + \xi$ with $\xi = O(1)$, these equations take the form

$$\frac{\mathrm{d}u}{\mathrm{d}\xi} = \left(\frac{n\mathscr{G}'(\xi) + ky_0^2\mathscr{F}''/\sqrt{2}}{y_0^2\phi} - \frac{1}{y_0+\xi}\right)u + \frac{n^2+k^2y_0^2}{y_0^2\phi}\mathrm{i}p, \tag{4.1}$$

$$\frac{\mathrm{d}p}{\mathrm{d}\xi} = \mathrm{i}\left(\frac{(\mathscr{G}^2)'}{y_0^3\phi} - \phi\right)u - \frac{2n\mathscr{G}}{y_0^3\phi}p, \tag{4.2}$$

$$\phi = k(\mathscr{F}'/\sqrt{2} - c) + n\mathscr{G}/y_0^2, \tag{4.3}$$

where in most places y_0 has been written for $y_0+\xi$ as a consistent leading-order approximation. As a result, for large y_0, the leading-order terms in an asymptotic expansion of the eigenfunctions, in inverse powers of y_0, obey the equations

$$\frac{\mathrm{d}u}{\mathrm{d}\xi} = \frac{\phi_0'}{\phi_0}u + \frac{\mathrm{i}k^2}{\phi_0}p, \tag{4.4a}$$

$$\frac{\mathrm{d}p}{\mathrm{d}\xi} = -\mathrm{i}\phi_0 u, \tag{4.4b}$$

$$\phi_0 = k(\mathscr{F}_0'/\sqrt{2}-c), \tag{4.4c}$$

with the basic profile $\mathscr{F}_0'$ given by (3.22). This is *precisely* the stability problem for the Bickley jet: see Drazin & Reid (1981, p. 233 ff). Hence we may conclude that, for k of $O(1)$, the sinuous and varicose two-dimensional instability modes of the Bickley jet appear as the dominant instability modes for the large-M Type II vortex under study here, as indeed might be expected physically. The swirl of the vortex and its motion inside and outside the ring-jet exert little influence.

Briefly, for background, the Bickley jet is known to have two unstable inertial modes: a 'varicose' and a 'sinuous' mode. The varicose mode exists for all non-zero wavenumbers, k, below $4\sqrt{2}$, and the sinuous mode for values of k less than $8\sqrt{2}$. The imaginary part of c vanishes at those end-point values of k, with peak growth rates (kc_1) occurring at k-values near $2\sqrt{2}$ and $4\sqrt{2}$ respectively. More details may be found in Drazin & Howard (1966) and Drazin & Reid (1981).

On the other hand, (4.4) would not be expected to represent the proper large-M limit of (4.1)–(4.3) for all wavenumbers k, especially for small k where the three-dimensional effects from the swirl and the larger-scale motion of the vortex might be expected to reassert themselves. In this section, therefore, we explore the modification of the sinuous Bickley mode for this vortex as the wavenumber k decreases. In §5, the process of modification is repeated for the varicose Bickley mode. For convenience the terms 'sinuous' and 'varicose' below refer to modes that are linked with the sinuous and varicose modes of the Bickley jet, in turn, when $k = O(1)$.

As k decreases, three major regimes of significant modification are found to emerge and these are investigated in turn in (*a*)–(*c*) below. Comments on them and comparisons are presented at the end of the section.

(*a*) *The first three-dimensional regime:* $k = O(y_0^{-1})$

The first new regime arises where k is decreased to the order of M^{-1}, i.e. $O(y_0^{-1})$ from §3. At this stage, the axial wavelength rises to become of the same order of the vortex width, and so the helical nature of the instability mode becomes important, unlike in the two-dimensional Bickley-jet instability alone. The appropriate scalings $k = \alpha y_0^{-1}$, $c = y_0^{-\frac{1}{2}}\hat{c}$, and $p = y_0^{-\frac{1}{2}}P$ lead to the new leading-order outer form of (4.1)–(4.3) for the instability properties holding away from the ring jet, namely

$$\frac{\mathrm{d}(Yu)}{\mathrm{d}Y} = \mathrm{i}\frac{n^2+\alpha^2Y^2}{-\alpha\hat{c}Y}P, \tag{4.5a}$$

$$\frac{\mathrm{d}P}{\mathrm{d}Y} = \mathrm{i}\alpha\hat{c}u, \tag{4.5b}$$

with σ and the as-yet unknown $\hat{c}$ of order one. The relevant perturbation solution here is

$$P = \begin{cases} I_n(\alpha Y), & Y < 1, \quad (4.6a) \\ BK_n(\alpha Y), & Y > 1, \quad (4.6b) \end{cases}$$

where I_n and K_n are modified Bessel functions of the first and second kind, B is a constant, while u is then given by (4.5*b*). These solutions holding outside the jet must be matched through the instability properties applying inside the jet.

In the inner region, i.e. within the jet, we let $\phi = y_0\hat{\phi}$, and expand u and $\hat{\phi}$ in inverse powers of $y_0^{\frac{1}{2}}$ as implied by the controlling equations. Then it is found that $\hat{\phi}_0 = \alpha\mathscr{F}'/\sqrt{2}$, $\hat{\phi}_1 = -\alpha\hat{c}$. The appropriate instability equations in the jet are therefore

$$\frac{\mathrm{d}u}{\mathrm{d}\xi} = \frac{n\mathscr{G}' + \alpha y_0 \mathscr{F}''/\sqrt{2}}{y_0\hat{\phi}} u + \mathrm{i}\frac{n^2+\alpha^2}{y_0\hat{\phi}} p, \quad (4.7a)$$

$$\frac{\mathrm{d}p}{\mathrm{d}\xi} = -\frac{\mathrm{i}\hat{\phi}}{y_0} u - \frac{2n\mathscr{G}}{y_0^2\hat{\phi}} p, \quad (4.7b)$$

in addition to some higher-order terms. Since $u_0 = C_1\hat{\phi}_0$, it follows that

$$\frac{\mathrm{d}p_0}{\mathrm{d}\xi} = -\frac{\mathrm{i}}{y_0} C_1 \hat{\phi}_0^2, \quad (4.8)$$

C_1 a constant, completing the leading instability term. Next, the u_1 equation, obtained from (4.7*a*), may then be integrated to give

$$u_1 = C_2\hat{\phi}_0 - \alpha\hat{c}C_1, \quad (4.9)$$

with C_2 a constant. The pressure and velocities in this thin inner region must now be matched at large $|\xi|$ with the outer solutions (4.6) at $Y = \pm 1$. Since $\hat{\phi}_0 \to 0$ for $|\xi| \to \infty$, $u_0 \to 0$, however, and hence the leading-order behaviour simply gives $u \sim -\alpha\hat{c}C_1/y_0^{\frac{1}{2}}$. This implies that the outer perturbation velocity must be continuous across $Y = 1$. Using (4.6) and (4.5*a*), we have then the result that the outer pressure gradient $\mathrm{d}P/\mathrm{d}Y$ must be continuous across $Y = 1$, giving the requirement that

$$I_n'(\alpha) = BK_n'(\alpha). \quad (4.10a)$$

On the other hand, (4.8) shows that there is a small jump, denoted by [ ], in the pressure itself across the inner region, of the form,

$$[p] = -\frac{\mathrm{i}}{y_0} C_1 \int_{-\infty}^{\infty} \hat{\phi}_0^2 \,\mathrm{d}\xi.$$

Further, for $\xi \to -\infty$, $u \sim -C_1\alpha\hat{c}/y_0^{\frac{1}{2}}$, and so this pressure-jump condition may be rewritten as

$$\hat{c}^2\,[P] = \frac{1}{2}\frac{\mathrm{d}P}{\mathrm{d}Y}\left[\int_{-\infty}^{\infty} (\mathscr{F}')^2 \,\mathrm{d}\xi\right] \quad \text{at} \quad Y = 1. \quad (4.10b)$$

Substitution of (4.6) into (4.10*b*), and utilizing (4.10*a*), therefore leads to the required formula for the scaled complex wave speed (and hence the growth rate)

$$\hat{c}^2 = \frac{\alpha^2\sqrt{2}}{12} I_n'(\alpha) K_n'(\alpha). \quad (4.11)$$

As a check in the present regime, the result (4.11) for $\hat{c}^2$ behaves like $-\alpha/12\sqrt{2}$ at large α, i.e. the wave speed $\hat{c}$ is purely imaginary then, to the first approximation,

thus yielding instability, in agreement with the small-k result in Drazin & Reid (1981) for the sinuous Bickley mode. Thus, the result (4.11) matches as required with the earlier two-dimensional solution.

The result (4.11) represents the main modification that occurs during this regime, due to the vortex effect. Even though the three-dimensional character of the disturbances is now evident, however, the presence of the angular velocity is not yet significant to the instability mode, a feature which leads to the subsequent stage.

(b) The second three-dimensional regime: $k = O(y_0^{-\frac{3}{2}})$

As k continues to drop, the analysis in the previous section eventually breaks down because the azimuthal convection of the velocity perturbations due to the relatively small swirling motion in the vortex becomes as important as the axial convection. It happens that this occurs when $k = O(y_0^{-\frac{3}{2}})$, as may be verified from an order-of-magnitude argument. So in this new regime we put $k = y_0^{-\frac{3}{2}}\beta$ with β of order unity, and it is appropriate to set $c = y_0^{-\frac{1}{2}}\hat{c}$ as before, since from (4.11) it is evident that $\hat{c}$ remains $O(1)$ as $\alpha \to 0$. The outer solutions away from the ring jet for the instability problem in this case are simpler now than in the previous regime, viz.

$$u = \begin{cases} AY^{|n|-1}, & Y < 1, \\ BY^{-|n|-1}, & Y > 1, \end{cases} \tag{4.12a}$$

and

$$p = \frac{iy_0^{-1}}{|n|}\begin{cases} \beta\hat{c}AY^{|n|}, & Y < 1, \\ (nG/Y^2 - \beta\hat{c})BY^{-|n|}, & Y > 1. \end{cases} \tag{4.12b}$$

These in effect replace the solutions (4.6a, b) in the previous range. We observe that along with the solutions in (4.12a) the basic swirl is $G = 0$ for $Y < 1$ and $G = 1$ for $Y > 1$, from §3.

The substantial difference from the previous stage now arises in the inner region. An expansion of u in inverse powers of $y_0^{\frac{1}{2}}$ is appropriate as before, since the scalings still hold, and so

$$u = y_0^{\frac{1}{2}}u_0 + u_1 + \ldots,$$

say. That yields the balance

$$\frac{\mathrm{d}u_0}{\mathrm{d}\xi} = \frac{\tilde{\phi}_0'}{\tilde{\phi}_0}u_0$$

for the leading-order perturbation, where $\tilde{\phi}_0 = \beta\mathscr{F}'/\sqrt{2}$. This leads to $u_0 = C_1\tilde{\phi}_0$ as before, but the u_1 equation is now far more complex because $\tilde{\phi}_1 = n\mathscr{G} - \beta\hat{c}$ is non-trivial in the current regime, owing to the enhanced azimuthal convection (represented by the term $\mathscr{G}$). The u_1 equation is found to be

$$\frac{\mathrm{d}u_1}{\mathrm{d}\xi} = \frac{\tilde{\phi}_0'}{\tilde{\phi}_0}u_1 + \left(\frac{n\mathscr{G}'}{\tilde{\phi}_0} - \frac{\tilde{\phi}_0\tilde{\phi}_1}{\tilde{\phi}_0^2}\right)u_0, \tag{4.13}$$

which has the solution $u_1 = F(\xi)\,\phi_0$, where

$$F = C_1\left[\left(1 - \frac{1}{\sqrt{2}}\right)\frac{n\xi}{\beta} + \frac{4}{\beta}(\tfrac{1}{2}n - \beta\hat{c})\sinh^2(\xi_0) + 2\frac{n}{\beta}\sinh(\xi_0)\cosh(\xi_0)\right]. \tag{4.14}$$

From (4.14), it is clear that for matching purposes

$$\left.\begin{aligned} u &\sim (n - \beta\hat{c})\,C_1, \quad \xi \to \infty, \\ u &\sim -\beta\hat{c}C_1, \quad \xi \to -\infty. \end{aligned}\right\} \tag{4.15}$$

In addition, the pressure equation (4.2) in this layer becomes

$$\frac{\mathrm{d}p}{\mathrm{d}\xi} = y_0^{-\frac{3}{2}}\mathrm{i}\left(\frac{(\mathscr{G}^2)'}{\phi_0} - \phi_0\right)u.$$

Hence the changes in the pressure across the inner ring-jet layer are related not only to the axial but also to the azimuthal momentum flux, another new feature in the current stage. Substituting for u_0 and integrating with respect to ξ, we find the pressure jump to be

$$\begin{aligned}[p] &= \mathrm{i}C_1 y_0^{-1}\left(1 - \int_{-\infty}^{\infty} \hat{\phi}_0^2\,\mathrm{d}\xi\right) \\ &= \mathrm{i}C_1 y_0^{-1}\left(1 - \frac{\sqrt{2}}{12}\beta^2\right). \end{aligned} \tag{4.16}$$

In consequence, the matching of the velocities (4.15) with the outer solutions (4.12*a*) and the joining of the pressures by means of (4.16) gives the scaled complex wave speed for this unstable mode, namely,

$$\beta\hat{c} = \tfrac{1}{2}n + \mathrm{i}\left[\tfrac{1}{4}n^2 - \tfrac{1}{2}|n|\left(1 - \frac{\sqrt{2}}{12}\beta^2\right)\right]^{\frac{1}{2}}. \tag{4.17}$$

This represents the main result of the present regime. It may be verified that (4.17) matches onto the earlier result (4.11), for $\beta \to \infty$ and $\alpha \to 0$ respectively, as required. At the other extreme, as k continues to decrease, the swirl velocity becomes dominant, and a final small-k regime is found to appear. This final regime is studied next.

(*c*) *The three-dimensional regime: $k = 0(y_0^{-2})$*

Guided by the behaviour of regime (*b*) at small β we find that a third new stage emerges when k is reduced to the order of y_0^{-2}. Let $k = y_0^{-2}\gamma$, say. Then the function ϕ of (4.3) is $O(y_0^{-2})$ at most, say $\phi = y_0^{-2}\Phi$, in the outer regions away from the ring jet. Next, supposing c remains $O(1)$, we see that (4.1) and (4.2) become

$$\frac{\mathrm{d}}{\mathrm{d}Y}(Yu) = \frac{\mathrm{i}n^2}{\Phi Y} y_0 p, \tag{4.18a}$$

$$\frac{\mathrm{d}p}{\mathrm{d}Y} + \frac{2n}{\Phi y^3} p = -\mathrm{i}\Phi\frac{u}{y_0}, \tag{4.18b}$$

respectively, in which Φ is $-\gamma c$ in $Y < 1$, but $n/Y^2 - \gamma c$ in $Y > 1$. In either case, the pressure perturbation function p can be shown to obey the same Cauchy–Euler equation as previously, so that the power-law solutions in (4.12*b*) still apply here, while u is now given by

$$u = \mathrm{i}y_0\frac{\mathrm{d}}{\mathrm{d}Y}\left(\frac{p}{\Phi}\right). \tag{4.19}$$

By contrast, the solution for u in the inner ring-jet region is, as previously, $u = C_1\tilde{\phi}$. Further, unlike before, the pressure equation (from (4.2)) in this wavenumber range includes only the effects of swirl and not those of the axial motion, within the jet region, and is specifically

$$y_0\frac{\mathrm{d}p}{\mathrm{d}\xi} = \mathrm{i}\frac{(\mathscr{G}^2)'}{\tilde{\phi}}u = \mathrm{i}C_1(\mathscr{G}^2)'.$$

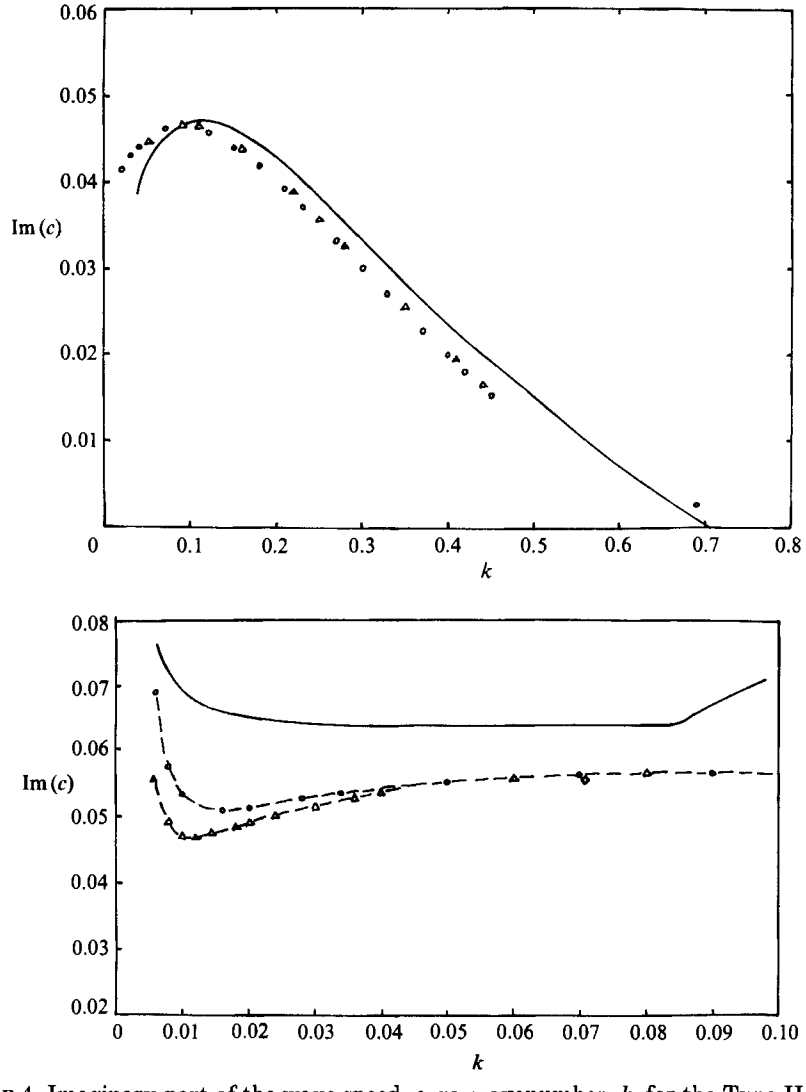

FIGURE 4. Imaginary part of the wave speed, c, *vs.* wavenumber, k, for the Type II sinuous mode, $M = 44.9$. (*a*) c_I *vs.* k. ○, $n = 3$; △, $n = -3$. Solid line is for the Bickley jet. (*b*) c_I *vs.* k at small k. ○, $n = 3$; △, $n = -3$. The solid line represents the asymptotic results from §4.

Thus, the pressure jump across the ring-jet layer follows as

$$[p] = \mathrm{i}\, C_1 y_0^{-1}. \tag{4.20}$$

Matching the inner perturbation-velocity solution $u = C_1 \tilde{\phi}$ to the outer perturbation u-form obtained from (4.19), and utilizing the corresponding perturbation-pressure results (4.20) and (4.12*b*) therefore leads to the principal result

$$\gamma c = \tfrac{1}{2}n + \mathrm{i}\,(\tfrac{1}{4}n^2 - \tfrac{1}{2}|n|)^{\frac{1}{2}} \tag{4.21}$$

for the complex wave speed c during the current regime. This matches at large γ with the small-β version of (4.17) as required.

So overall here we see that the sinuous modes in the present stage are characterized by an outer structure in which both the radial velocity and the pressure are

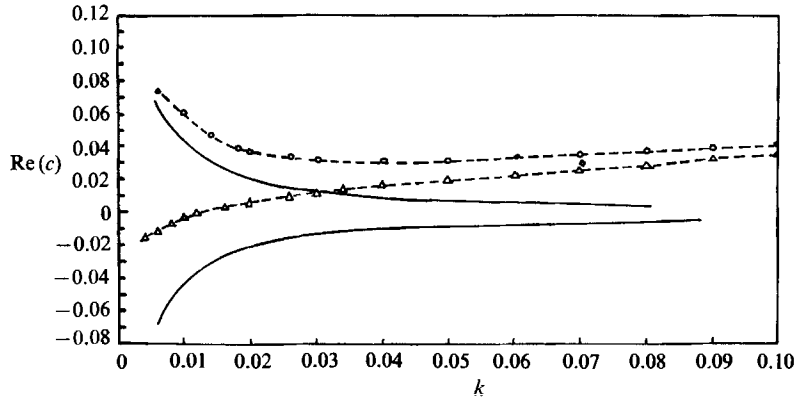

FIGURE 5. Real part of the wave speed, c, *vs.* wavenumber, k, for the Type II sinuous mode, $M = 44.9$, showing detail at small wavenumber. ○, $n = 3$; △, $n = -3$. The solid lines represent the asymptotic results from §4 for $n = \pm 3$.

discontinuous at $Y = 1$. The Bickley-jet structure holding in the vicinity of the cylindrical surface $Y = 1$ smooths out the instability eigenfunctions in a fashion dependent on the relative sizes of the azimuthal and axial convection of the disturbances due to the basic vortex flow. In particular, the pressure jump induced across the jet is determined by an integral of the following version of (4.2):

$$\frac{\mathrm{d}p}{\mathrm{d}\xi} = \mathrm{i}\left\{\underbrace{\frac{(\mathscr{G}^2)'}{y_0^3}}_{\text{[I]}} - \underbrace{\left[k\left(\frac{\mathscr{F}'}{\sqrt{2}} - c\right) + \frac{n\mathscr{G}}{y_0^2}\right]^2}_{\text{[II]}}\right\} C_1. \tag{4.22}$$

For the first regime (a) above, i.e. $k = 0(y_0^{-1})$ and larger, the contribution II dominates that of I, whereas for the second regime (b) where $k = O(y_0^{-\frac{3}{2}})$ both I and II matter; and for $k = O(y_0^{-2})$ in the third regme, (c), only the contribution I affects the pressure jump to leading order.

For the sake of comparisons with our numerical results, a multiplicative composite expression for main results (4.11), (4.17), and (4.20) above is used, giving

$$c = \frac{n}{2ky_0^2} + \mathrm{i}\left[\frac{\frac{1}{4}n^2 - \frac{1}{2}|n|}{k^2 y_0^4} - \frac{\sqrt{2}}{12} y_0 k^2 I_n'(ky_0) K_n'(ky_0)\right]^{\frac{1}{2}} \tag{4.23}$$

as the predicted complex wave speed. Figure 4 shows the variation of c_I predicted from (4.23) plotted *vs.* k for a flow-force value M of 44.9 (corresponding to $y_0 = 60.64$); alongside is the result of a fully numerical computation of c_I for this sinuous mode, without any large-M approximation. The details of the numerical procedure used here may be found in Duck & Foster (1980). Figure 5 shows c_R as well, for the same case. The agreement is not particularly close quantitatively, but we recall that the terms of next order in the c-series are only $O(y_0^{-\frac{1}{2}})$ smaller, and hence numerically are still substantial (about 13%) even at a y_0 of 60.64. Moreover, the diamond symbols in figure 4(b) and figure 5 are the results of retaining three terms in the long-wave expansion for the *Bickley jet* (Drazin & Howard 1966). They agree very well with the fully numerical work. In addition, the overall trends seem correct and there is good qualitative agreement between the asymptotic solutions presented in this section and the numerical results.

5. Type II 'varicose' inertial instability

As with the 'sinuous' modes of the previous section, the properties of 'varicose' instability modes at large flow force M divide into three distinct regimes (*a*)–(*c*) depending on the size of the wavenumber k, and these three unstable regimes, where k has the orders 1, y_0^{-1}, y_0^{-2} respectively, are considered in turn below.

(*a*) *The two-dimensional regime:* $y_0^{-1} \ll k \ll 1$

It was pointed out at the beginning of §4 that when k is $O(1)$, with the wave speed c and azimuthal wavenumber n also assumed to be $O(1)$, the stability problem of §§2, 3 reduces to solving for the two-dimensional inviscid stability of the Bickley jet concentrated near the cylindrical face $y = y_0$ so that the Rayleigh equation,

$$(\mathscr{W}-c)(\Psi''-k^2\Psi) = \mathscr{W}''\Psi, \tag{5.1a}$$

$$\Psi(O) = \Psi(\infty) = 0 \tag{5.1b}$$

holds then for the varicose modes, as well as for the sinuous modes of §4. Here ψ is the perturbation stream function and ξ is $O(1)$ with

$$y = y_0+\xi, \quad \mathscr{W} = a_1\,\mathrm{sech}^2(a_2(\xi+\sqrt{2})) \tag{5.1c}$$

where $\mathscr{W}$ is the basic axial-flow profile and $a_1 = 2^{-\frac{5}{2}}$, $a_2 = 2^{-\frac{3}{2}}$. The Bickley-jet instability features are well established, e.g. see Drazin & Reid (1981); of note here are two such features. First, instability is present for k less than a cut-off value $k = k_c$ (see however §6 in the context of the vortex instability there). Secondly, for long waves, as $k \to 0$, the wave speed $c \to a_1$ from below, so that the waves travel at virtually the maximum flow speed. Our concern is with the latter aspect, which involves a change in the structure of the varicose modes.

For small k the varicose-mode solution in fact splits into three zones I–III as shown in figure 6, and

$$c = a_1\,(1+k^{\frac{2}{3}}c_1+\ldots) \tag{5.2}$$

where the complex perturbation c_1 is to be found. The solution then develops as follows in zones II and III:

$$\Psi = \Psi_0+k^{\frac{2}{3}}\Psi_1+k\Psi_2+\ldots \tag{5.3a}$$

in II (where $\xi = O(1)$),

$$\Psi = k^{\frac{2}{3}}\hat{\Psi}_0+\ldots \tag{5.3b}$$

in III (where $\xi+\sqrt{2} = k^{\frac{1}{3}}\hat{\xi}$), with $\mathscr{W}(\xi)$ remaining $O(1)$ in the former but $\mathscr{W} = a_1 - a_1a_2^2k^{\frac{2}{3}}\hat{\xi}^2+\ldots$, in the latter zone which is focused near the position of the peak jet velocity, in the middle of the ring jet. The major cause of all the scalings in (5.2), (5.3*a*, *b*) is the thickness of this innermost central zone III, which acts to smooth out the discontinuities arising in the zone II just outside and whose extent is found to be $O(k^{\frac{1}{3}})$ from the orders of magnitude involved. Substituting into (5.1) we find the perturbation solutions

$$\Psi_0 = a_1^{-1}A_0(\mathscr{W}-a_1), \quad \Psi_1 = -a_1^{-1}A_0c_1, \tag{5.4a, b}$$

$$\Psi_2 = -B_2[\xi^*\tanh^2\xi^*-\tanh\xi^*-\tfrac{1}{2}\coth\xi^*] \tag{5.4c}$$

and

$$\hat{\Psi}_0 = \hat{B}_0[(\hat{\xi}^2+\hat{c}_1)\tan^{-1}(\hat{\xi}/\hat{c}_1^{\frac{1}{2}})+\hat{c}_1^{\frac{1}{2}}\hat{\xi}]/a_2^{\frac{2}{3}}, \tag{5.5}$$

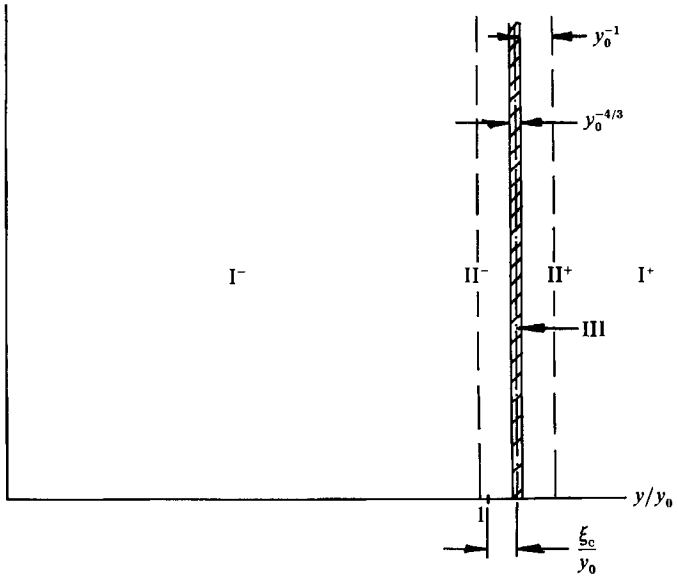

FIGURE 6. Schematic of the five regons of the eigenfunction for the three-dimensional varicose modes for Long's vortex. The scales shown are for the second three-dimensional regime of §5; the structure is the same for all long-wave varicose modes, but the detailed scales vary with the wavenumber order.

where $\xi^* = a_2\xi$, $\hat{\xi} = a_2^{\frac{4}{3}}\xi$, $\hat{c}_1 = a_2^{\frac{2}{3}}c_1$. The matching between the zones II, III then fixes the constants B_2, B_0 in terms of A_0:

$$\hat{B}_0 = -2A_0/\pi, \quad B_2 = -2\hat{B}_0 c_1^{\frac{2}{3}}. \tag{5.6a, b}$$

The outer zone I, however, of extent $O(k^{-1})$ in ξ, has essentially potential flow, so that there ψ is required to have the form $\exp(-k\xi)$ rather than $\exp(k\xi)$, to avoid exponential growth. Hence the large-ξ behaviour in zone II, i.e.

$$-A_0 - k^{\frac{2}{3}}A_0 c_1/a_1 - kB_2 a_2 \xi + \ldots$$

from (5.4), must be proportional to $1-k\xi+\ldots$ predominantly, implying that

$$a_2 B_2 = -A_0. \tag{5.6c}$$

Combining (5.6*a–c*) therefore we obtain the main result, for the complex wave speed correction, as

$$c_1 = (\pi/4a_2)^{\frac{2}{3}}\exp(\tfrac{1}{3}2\pi\mathrm{i}), \tag{5.7}$$

yielding $c_{1i} > 0$ and hence instability. This result agrees as required with the previous long-wave results of Drazin & Howard (1966) for two-dimensional jets although here the emphasis is put more on the structural changes at small wavenumbers since these provide the basis for the next significant regime studied in (*b*) below. Zone I above, the outermost zone, is a region of negligible basic flow in effect, while zone II merely induces a displacement effect at leading order, bringing in the precise details of the basic-flow profile, and III is a critical layer, in some senses, with the basic velocity at its maximum. The singularity arising in the zone II solution (5.4*c*) as $\xi \to -\sqrt{2}$ is smoothed out by the thin zone III, and ψ is then odd in ξ_0. The structure above points to the following stage next.

(*b*) *The first three-dimensional regime: $k = O(y_0^{-1})$*

Here k is reduced to $O(y_0^{-1})$, say $k = y_0^{-1}\alpha$. The reason for this regime arising is that the outermost zone I above, of extent $O(k^{-1})$ expands right across the gap between the ring jet and the symmetry axis, producing a new three-dimensional influence. Again three different zones are present, labelled I–III by analogy with those in (*a*), although here we use the disturbance velocities and pressures in each zone to draw out more clearly the major physical balances present. These also require fewer terms in the expansions, incidentally. In the current regime, as implied by the earlier expansions, we have

$$c = c_0 + y_0^{-\frac{2}{3}} c_1 + \ldots, \tag{5.8}$$

where c_0 is real, and turns out to be equal to a_1, whereas c_1 is found subsequently to be complex. Zone I is then the largest one, where $y = y_0 Y$ with Y of $O(1)$ and the asymptotic expansions begin as

$$(u, p) = (u^*, p^*) + \ldots, \quad (w, g) = (y_0^{-1} W, G) + \ldots, \tag{5.9a, b}$$

where the basic flow properties (W, G) are given by (3.16) and (3.19) and are functions of Y. For simplicity, we now drop the *-notation. So there $\phi = -y_0^{-1}\alpha c_0$ to leading order and the governing instability equations reduce to

$$\frac{\mathrm{d}u}{\mathrm{d}Y} = -\frac{u}{Y} - \mathrm{i}\frac{(n^2 + \alpha^2 Y^2)}{\alpha c_0 Y^2} p, \tag{5.9c}$$

$$\frac{\mathrm{d}p}{\mathrm{d}Y} = \mathrm{i}\alpha c_0 u. \tag{5.9d}$$

Thus the pressure perturbation satisfies the modified Bessel's equation

$$Y^2 \frac{\mathrm{d}^2 p}{\mathrm{d}Y^2} + Y\frac{\mathrm{d}p}{\mathrm{d}Y} - (n^2 + \alpha^2 Y^2) p = 0, \tag{5.10a}$$

and the appropriate boundary conditions become

$$p \text{ bounded at } Y = 0, \infty, \tag{5.10b}$$

$$p \text{ continuous}, \quad \frac{\mathrm{d}p}{\mathrm{d}Y} \text{discontinuous, at } Y = 1. \tag{5.10c}$$

Here the two constraints in (5.10*c*) anticipate the properties holding inside the ring jet close to $Y = 1$. Those properties come from the zones II, III.

In zone II we have $y = y_0 + \xi$ and, again from the previous scalings,

$$(u, p) = (u_0, p_0) + y_0^{-\frac{2}{3}}(u_1, p_1) + y_0^{-1}(u_2, p_2) + \ldots, \tag{5.11a}$$

$$(w, g) = (\mathscr{W}, \mathscr{G}) + \ldots. \tag{5.11b}$$

Here $\mathscr{W}$ and $\mathscr{G}$ are written for the basic axial velocity and circulation in the ring jet, from (3.20) and (3.21), and we have written here, for brevity, the quantity $\mathscr{W}$ for $\mathscr{F}'/\sqrt{2}$ and ξ is now of order unity. Then, the function $\phi = y_0^{-1}\alpha(\mathscr{W} - c_0) - y_0^{-\frac{5}{3}}\alpha c_1 + \mathrm{y}_0^{-2} n\mathscr{G} + \ldots$. The successive solutions are found to be simply the displacement-induced forms

$$u_0 = A_0(\mathscr{W} - c_0), \quad u_1 = -A_0 c_1, \tag{5.12a, b}$$

$$p_0 = \text{const.}, \quad p_1 = \text{const.} \tag{5.12c}$$

along with expressions for u_2, p_2 which need not concern us here. In (5.12) A_0 is a constant and the result $c_0 = a_1$ is required to allow the varicose solution to be continuous through the critical level where $\mathscr{W} = c_0$. Then the critical layer, zone III, lying near the point of maximum axial speed, has $y = y_0 - \sqrt{2} + y_0^{-\frac{1}{3}}\hat{y}$, with $\hat{y}$ of order unity, and the scales above imply that the expansions

$$u = y_0^{-\frac{2}{3}}\hat{u}_0 + \ldots, \quad p = \hat{p}_0 + \text{consts.} + y_0^{-\frac{5}{3}}\hat{p}_* + \ldots \tag{5.13a, b}$$

$$\mathscr{W} = a_1 - \lambda y_0^{-\frac{2}{3}}\hat{y} + \ldots, \quad \mathscr{G} = \mathscr{G}_0 + y_0^{-\frac{1}{3}}\mathscr{G}_1\hat{y} + \ldots \tag{5.13c, d}$$

hold, where $(\mathscr{G}_0, \mathscr{G}_1)$ are constants and $\phi \sim -\alpha(\lambda\hat{y}^2 + c_1)\, y_0^{-\frac{5}{3}}$, $\lambda = a_1 a_2^2$. So the main governing equation here turns out to be

$$\frac{\mathrm{d}\hat{u}_0}{\mathrm{d}\hat{y}} = \frac{2\lambda\hat{y}\hat{u}_0}{\lambda\hat{y}^2 + c_1} - \mathrm{i}\frac{(n^2+\alpha^2)}{\alpha(\lambda\hat{y}^2 + c_1)}\hat{p}_0, \tag{5.14a}$$

with $\hat{p}_0$ a constant. This yields the local solution

$$\hat{u}_0 = \frac{-\mathrm{i}(n^2+\alpha^2)\,\hat{p}_0}{2\alpha(\lambda c_1^3)^{\frac{1}{2}}}\left[(\lambda\hat{y}^2 + c_1)\tan^{-1}\left(\frac{\lambda\hat{y}}{c_1}\right)^{\frac{1}{2}} + (\lambda c_1)^{\frac{1}{2}}\hat{y}\right] + \hat{B}_0(\lambda\hat{y}^2 + c_1), \tag{5.14b}$$

where the match with zone III outside determines the constants appearing, in the form

$$\mp\mathrm{i}(n^2+\alpha^2)\,\hat{p}_0/(4\alpha(\lambda c_1^3)^{\frac{1}{2}}) + \hat{B}_0 = -A_0^{\pm}. \tag{5.15}$$

The superscripts $\pm$ refer to evaluation in zone II for $\xi \gtrless 0$ respectively: see figure 6.

The above properties in the thinner zones $\mathrm{II}^{\pm}$, III therefore lead to the jump conditions on the external pressure and its gradients, viz. the perturbation velocity u in zones $\mathrm{I}^{\pm}$ as $Y \to 1\pm$ in turn, namely

$$p^+ = p^- = \hat{p}_0 \quad \text{at} \quad Y = 1, \tag{5.16a, b}$$

$$u^{\pm} = -a_1 A_0^{\pm} \quad \text{at} \quad Y = 1. \tag{5.16c, d}$$

Consequently the split solution

$$p^- = \sigma I_n(\alpha Y), \quad p^+ = \sigma K_n(\alpha Y)\, I_n(\alpha)/K_n(\alpha) \tag{5.17a, b}$$

holds, from (5.10). So (5.15) then yields the required eigenrelation fixing the main complex wave-speed term c_1 as

$$c_1 = \left[\frac{(n^2+\alpha^2)\,\pi}{2\alpha a_2}\left(\frac{I_n'(\alpha)}{I_n(\alpha)} - \frac{K_n'(\alpha)}{K_n(\alpha)}\right)\right]^{\frac{2}{3}} a_1 \exp(\tfrac{2}{3}\pi\mathrm{i}), \tag{5.18}$$

since, from (5.9*d*), $u^{\pm} = (\mathrm{d}p^{\pm}/\mathrm{d}Y)/\mathrm{i}\alpha c_0$ in the outer zones $\mathrm{I}^{\pm}$.

As a check, for large α in (5.18), $K_n'/K_n \to -1$, $I_n'/I_n \to 1$ and in consequence $c_1 \sim (|n|\pi/4a_2)^{\frac{2}{3}}\exp(\frac{2}{3}\pi\mathrm{i})$ for any finite n, joining with the previous two-dimensional regime (*a*) (see (5.7)), as required. For small α on the other hand, which is the other extreme of most interest, $K_n(\alpha) \sim \alpha^{-|n|}$, $I_n(\alpha) \sim \alpha^{|n|}$ for finite α and any $|n| \neq 0$, so that then c_1 levels out at the $O(1)$-value,

$$c_1 \sim (n\pi/4a_2)^{\frac{2}{3}}\exp(\tfrac{2}{3}\pi\mathrm{i}) \quad \text{as} \quad \alpha \to 0. \tag{5.19}$$

This result guides the subsequent analysis in regime (*c*), for smaller α-values, such as extra regime being expected anyway since the swirl velocity has played no significant part so far, e.g. in the derivation of (5.18). The nature of zones I and II suggests that the swirl enters the reckoning when k drops to $O(y_0^{-1})$, which indeed defines the new stage (*c*) below where k is reduced to the order of y_0^{-2}. Meanwhile, we note that for

the current unstable three-dimensional regime the widest zone, I, has effectively no basic flow and so the disturbances have potential-flow properties, but now in three dimensions, while zone II covering most of the ring jet is altered little from its form in the earlier stage (*a*), with the swirl, the cross-stream pressure gradient and three-dimensionality have only higher-order influences. The thinnest zone III suffers three-dimensional effects, however, through the term n^2 in (5.14). All the three zones involved interact strongly. Again, as for the sinuous case, the term 'varicose' loses some physical meaning here since for instance the pressure gradient is no longer odd about $\xi = 0$, although as remarked earlier the present unstable modes stem from continuation of the earlier unstable varicose two-dimensional branch.

(*c*) *The second three-dimensional regime:* $k = O(y_0^{-1})$

Here, as anticipated, $k = y_0^{-2}\beta$ is of order y_0^{-2}, and consequently

$$c = c_0 + y_0^{-\frac{2}{3}} c_1 + \ldots \tag{5.20}$$

and the swirl comes strongly to the fore. As a result the critical layer III is found to move off-centre in the jet, with $c_0 \neq a_1$ now. The scales involved throughout this regime again follow from the previous ones.

The outermost zone I has $Y = y_0^{-1} y$ of $O(1)$ again, but

$$(u, p) = (u^*, y_0^{-1} p^*) + \ldots, \tag{5.21a}$$

$$\phi = y_0^{-2} \Phi, \quad \text{where} \quad \Phi = -\beta c_0 + nG/Y^2, \tag{5.21b}$$

where G is 1 in $Y > 1$ but zero in $Y < 1$. Therefore the controlling instability equations here are

$$\frac{\mathrm{d}u^*}{\mathrm{d}Y} = -\frac{u^*}{Y} + \mathrm{i}\frac{n^2 p^*}{Y^2 \Phi}, \tag{5.22a}$$

$$\frac{\mathrm{d}p^*}{\mathrm{d}Y} = -\mathrm{i}\Phi u^* - \frac{2nGp^*}{Y^3 \Phi}, \tag{5.22b}$$

for which the solutions are

$$p^{*-} = q^- Y^{|n|}, \qquad u^{*-} = -\mathrm{i}q^- |n| Y^{|n|-1}/\beta c_0, \tag{5.23a, b}$$

$$p^{*+} = q^+ (n/Y^2 - \beta c_0)\, Y^{-|n|}, \quad u^{*+} = -\mathrm{i}q^+ |n| Y^{-|n|-1}, \tag{5.23c, d}$$

where the constants (q^+, q^-) are unknown. The jump conditions at $Y = 1 \pm$ required to fix the solution above emerge again from the solution features in the inner zones II, III covering the ring jet.

In zone II, $\xi = y - y_0$ is the relevant coordinate again and

$$(u, p) = (u_0, y_0^{-1} p_0) + \ldots, \tag{5.24a}$$

$$\phi \sim y_0^{-2} [\beta(\mathscr{W} - c_0) + n\mathscr{G}], \tag{5.24b}$$

so that the swirl becomes important here also. The governing equations produced by the expansions here then provide the solutions

$$u_0^{\pm} = \beta^{-1} A_0^{\pm} [\beta(\mathscr{W} - c_0) + n\mathscr{G}], \tag{5.25a}$$

$$p_0^{\pm} = \Pi^{\pm} + \mathrm{i} A_0^{\pm} \mathscr{G}^2/\beta \tag{5.25b}$$

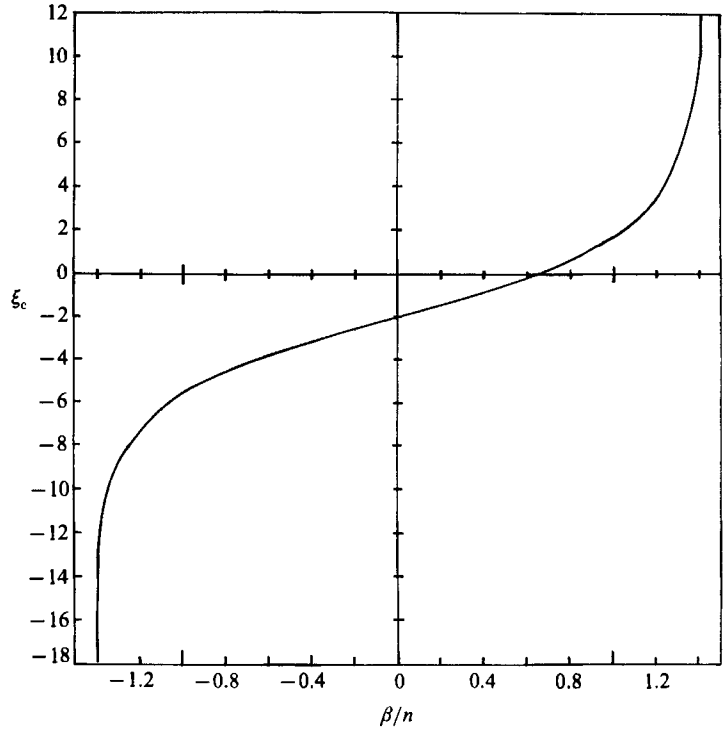

FIGURE 7. Location of the critical layer III for the second three-dimensional varicose mode (§5(*c*)) for Long's vortex.

on either side of the critical layer, with $A_0^{\pm}, \Pi^{\pm}$ being constants and the terms involving $\mathscr{G}$ representing new swirl-velocity effects, as anticipated. The critical layer III occurs where both u_0 and u_0' reach zero, which leads to the two equations

$$\beta(\mathscr{W}-c_0)+n\mathscr{G}=0 \quad \text{at} \quad \xi=\xi_c, \tag{5.26a}$$

$$\beta\mathscr{W}'+n\mathscr{G}'=0 \quad \text{at} \quad \xi=\xi_c, \tag{5.26b}$$

for the unknown critical position ξ_c and wave speed c_0. In general, $\xi_c \neq 0$ now and so the critical layer III is moved off-centre, compared with the two previous régimes, as shown in figure 7, this movement being inwards (outwards) for positive (negative) n. Inside this critical layer III we have $y = y_0+\xi_c+y_0^{-\frac{1}{3}}\hat{y}$, implying the expressions

$$(u,p) = (y_0^{-\frac{2}{3}}\hat{u}_0, y_0^{-1}\hat{p}_0)+\ldots, \tag{5.27a}$$

$$\mathscr{W} = \mathscr{W}_0+y_0^{-\frac{1}{3}}\hat{y}\mathscr{W}_1-y_0^{-\frac{2}{3}}\hat{y}^2\mathscr{W}_2+\ldots, \tag{5.27b}$$

$$\mathscr{G} = \mathscr{G}_0+y_0^{-\frac{1}{3}}\hat{y}\mathscr{G}_1-y_0^{-\frac{2}{3}}\hat{y}^2\mathscr{G}_2+\ldots, \tag{5.27c}$$

where $(\mathscr{W}_0, \mathscr{W}_1, \mathscr{W}_2)$ and $(\mathscr{G}_0, \mathscr{G}_1, \mathscr{G}_2)$ are constants, related by equations obtained from the relations (5.26), namely $\beta(\mathscr{W}_0-c_0)+n\mathscr{G}_0=0$, $\beta\mathscr{W}_1+n\mathscr{G}_1=0$. Thus $\phi \sim y_0^{\frac{8}{3}}\Phi$ say and we find that the solution here has

$$\frac{\hat{u}_0}{\Phi} = \frac{\mathrm{i}n^2\hat{p}_0}{2(\beta\mathscr{W}_2-n\mathscr{G}_2)^{\frac{1}{2}}(\beta c_1)^{\frac{3}{2}}}\langle\,\rangle+\hat{B}_0, \tag{5.28}$$

after some working, with $\hat{p}_0$ = constant and with the term in angled brackets being analogous with that in (5.14*b*). Also here the term $\Phi = -\beta(\hat{y}^2\mathscr{W}_2+c_1)+n\mathscr{G}_2\hat{y}^2$ once more brings in the influence of the swirl of the basic vortex.

The required matching of the velocities and pressures between the zones II, III then yields the two relations

$$\beta^{-1}A^{\mp}(-\beta\mathscr{W}_2+n\mathscr{G}_2)=\pm n^2\hat{p}_0(\beta\mathscr{W}_2-n\mathscr{G}_2)^{\frac{1}{2}}\tfrac{1}{4}\pi(\beta c_1)^{\frac{3}{2}}+\Gamma\hat{B}_0, \qquad (5.29a,b)$$

$$\hat{p}_0=\Pi^{\pm}+\mathrm{i}\beta^{-1}A_0^{\pm}\mathscr{G}_0^2, \qquad (5.29c,d)$$

where Γ is a constant. In turn, the velocity and pressure match between the zones I, II provides the missing jump conditions for the power-law outer solutions (5.23):

$$\frac{\mathrm{i}|n|q^-}{\beta c_0}=c_0A_0^-, \quad \mathrm{i}|n|q^+=\beta^{-1}A_0^+(\beta c_0-n), \qquad (5.29e,f)$$

$$(n-\beta c_0)q^+=\Pi^++\mathrm{i}\beta^{-1}A_0^+, \quad q^-=\Pi^-. \qquad (5.29g,h)$$

Hence, combining (5.29*a–h*) we obtain the main eigenrelation

$$\tfrac{1}{2}n^2\pi\left[\frac{(n-\beta c_0)^2}{|n|}+\mathscr{G}_0^2-1\right]\left[\frac{\beta^2c_0^2}{|n|}-\mathscr{G}_0^2\right]=\left[1-\frac{\beta^2c_0^2}{|n|}-\frac{(n-\beta c_0)^2}{|n|}\right](\beta\mathscr{W}_2-n\mathscr{G}_2)^{\frac{1}{2}}(\beta c_1)^{\frac{3}{2}} \qquad (5.30)$$

which determines the complex wave-speed contribution c_1 for given wavenumbers β, n.

With the forms for $\mathscr{W}$ and $\mathscr{G}$ given in §3, the relation (5.26*b*) may be solved to determine the location of the critical point, given by

$$\tanh(\xi_c/2^{\frac{3}{2}}+\tfrac{1}{2})=n/(4\beta a_1), \qquad (5.31a)$$

with the wave speed c_0 then determined from (5.26*a*) to be

$$c_0=a_1(1+n/(4\beta a_1))^2. \qquad (5.31b)$$

From these properties we note that, since c_0 is real and positive, modes with positive azimuthal wavenumber n are 'prograde', i.e. those modes propagate around the vortex in the same direction as the swirl in the basic flow; any $n<0$ modes are similarly labelled 'retrograde'. Further, the structure remains intact only for $\beta>\beta_c$, where the cutoff value is

$$\beta_c=|n|/4a_1. \qquad (5.31c)$$

As $\beta\to\beta_c$ from above, the critical position $|\xi_c|\to\infty$, and so the critical layer III in effect begins to leave the ring-jet zone II, moving toward the outermost regions $I^{\pm}$ for $n\gtrless 0$, with the wave speed $c_0\sim[n+|n|]/(2\beta_c)$ at that stage. The square-root term $(\beta\mathscr{W}_2-n\mathscr{G}_2)^{\frac{1}{2}}$ in (5.30) is real throughout the range $\beta>\beta_c$, since $\mathscr{W}_2=\frac{1}{2}\mathscr{W}''(\xi_c)$, $\mathscr{G}_2=\frac{1}{2}\mathscr{G}''(\xi_c)$, giving $\beta\mathscr{W}_2-n\mathscr{G}_2=a_2^2\beta a_1(1-n^2/4\beta^2a_1^2)^2$, which is positive above β_c. As a check, we note that for increasingly large β we have c_0 retreating to the value a_1, and (5.30) shows that then $c_1^{\frac{3}{2}}\to-|n|a_1^{\frac{3}{2}}/4a_2$, merging with the previous three-dimensional regime (*b*) as required (see (5.19)).

For further discussion, it is more convenient to write (5.30) explicitly in terms of n and β,

$$\pi\left(1-\frac{n^2}{16\beta^2a_1^2}\right)[(\beta a_1-\tfrac{1}{4}n)^2+\tfrac{1}{4}|n|][(\beta a_1+\tfrac{1}{4}n)^2-\tfrac{1}{4}|n|]$$

$$=2a_2(\beta a_1)^{\frac{1}{2}}(\beta c_1)^{\frac{3}{2}}\left(1+\frac{n^2}{16\beta^2a_1^2}\right)^{\frac{1}{2}}\left[1-\tfrac{1}{2}|n|\left(1+\frac{1}{4}\left(\frac{n}{4\beta a_1}+\frac{4\beta a_1}{n}\right)^2\right)\right], \qquad (5.32)$$

on use of (5.31).

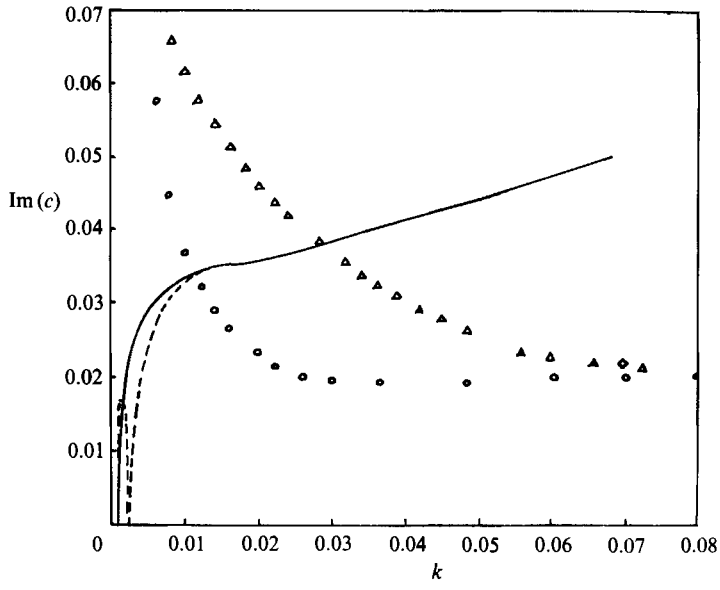

FIGURE 8. Imaginary part of the wave speed, c, *vs.* wavenumber, k, for the Type II varicose mode, $M = 44.9$ at small k. ○, $n = 3$; △, $n = -3$. The solid line represents the asymptotic result from §5 for $n = 3$; the broken line, the asymptote for $n = -3$.

The principal aspects of this three-dimensional interactive regime (c), then, are quite different for $n > 0$ and $n < 0$ modes. The $n > 0$ ones are prograde; the $n < 0$ modes are retrograde. As β decreases toward β_c, in addition, the prograde and retrograde modes diverge, c_0 rising to $4a_1$ ($n > 0$) or falling to O ($n < 0$), as noted already above. As $\beta \to \beta_c^+$, the approximate behaviour of (5.32) is

$$(\beta c_1)^{\frac{3}{2}} \sim -\frac{\pi a_1^2}{a_2 \sqrt{2|n|}} (n-1) \frac{\beta^2 - \beta_c^2}{|n|-1}, \tag{5.33}$$

so that c_I vanishes to first and second order at β_c, independent of the sign of n.

It is evident from (5.32) that the terms in the second square bracket on the left side of (5.32) may vanish, and that turns out to be possible for $n < 0$ modes only; hence $\beta c_1 \to 0$ for $\beta \to \beta^*$ as well, where β^* is seen to be $(\frac{1}{2}(-n)^{\frac{1}{2}} - \frac{1}{4}n)/a_1 = (1 + 2/(-n)^{\frac{1}{2}})\beta_c$. If we write $\beta^* a_1 = -(\frac{1}{4}n)\kappa$, then near β^* (5.32) takes the approximate form

$$(\beta c_1)^{\frac{3}{2}} \sim \frac{-\pi n}{4a_2} \frac{(1-\kappa^2)(1-\frac{1}{4}n(\kappa+1)^2)(\beta-\beta^*)a_1}{\kappa^{\frac{3}{2}}(\kappa^2+1)^{\frac{1}{2}}(-1-\frac{1}{8}n(\kappa^2+1/\kappa^2+6))}. \tag{5.34}$$

So $c_1 \to 0$ as $\beta \to \beta_c^+$ for both $n > 0$ and $n < 0$ modes, and also $c_1 \to 0$ as $\beta \to \beta^*$ for the retrograde mode ($n < 0$) only. Figure 8 shows c_{1I} *vs.* k for the examples $n = \pm 3$.

Computational comparisons are described in the following section.

6. Further discussion

We finish with a number of points concerning both the 'sinuous' and 'varicose' modes for this vortex.

Regarding the varicose modes first, the upper cut-off beyond k_c in regime (a) brings the swirl back into action again. That delays the cut-off to a value of k higher than

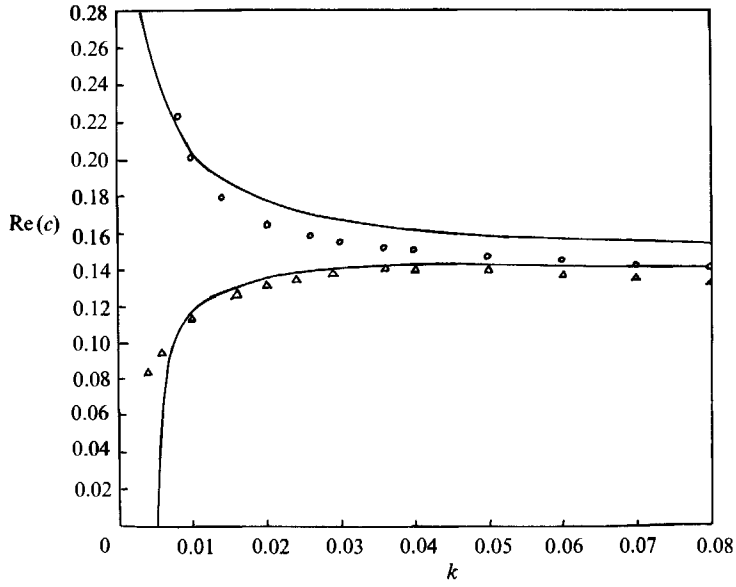

FIGURE 9. Real part of the wave speed, c, *vs.* wavenumber, k, for the Type II varicose mode, $M = 44.9$ at small k. ○, $n = 3$; △, $n = -3$. The solid lines represent the asymptotic results from §5.

that for the Bickley jet, as described in the Appendix, while the lower cut-off(s) suggested during regime (*c*) have been discussed in the previous section.

Computational studies for large finite values of M are described in §4 for the sinuous modes, where reasonable agreement with the current theory is found at least in a qualitative sense. The same numerical method was applied to the varicose modes yielding the results and comparisons shown in figures 8 and 9. Here the agreement is less overall. For instance, the theory of §5 and the computations agree fairly well on the variation of c_R with k for $n = \pm 3$, but not at all for c_I for either $n = 3$ or $n = -3$. Increasing the values of the effective flow force M used in the computation shows a trend not inconsistent with the theory, but it appears that the overall comparisons, certainly in quantitative terms, are hindered by the large relative corrections in the theory, the insufficiently large values of M and/or the outer edge $y = y_{edge}$ taken in the computations, and/or possible mode-jumping in the numerical work.

As a check on the matter of the vortex-edge effects at a finite radius, the vortex edge in the computations was extended by 60%. This extension produced changes in c_R and c_I only in the third decimal place. Even more surprising, the eigenfunction itself showed virtually no change. The reason for this is that the edge boundary condition employed in the computations, as stated in Duck & Foster (1980), is $p + icu = 0$. That choice, originally recorded in Burggraf & Foster (1977*a*), fortunately picks out the required K_n behaviour of the eigenfunction for large r, and suppresses the undesired I_n behaviour. Additionally, the analyses of §§4 and 5 may be repeated for an edge at a finite value of Y, say Y_1; such analyses show no qualitative change in the long-wave results for the varicose mode. In particular, the zeros of c_I at $\beta = \beta_c$ and at $\beta = \beta^*$ are still there at the same locations. Only the derivative of c_I at these zeros is slightly altered.

We move on therefore to the mode-jumping aspect. Leibovich & Stewartson (1983) discuss at length the difficulty of obtaining near-neutral eigensolutions by numerical

means for the Batchelor vortex. Our difficulties here are virtually identical. Briefly, the numerical results are obtained by using a converged wave speed at a particular (small) k as a starting value, decrementing k by a small amount, and computing the wave speed at the new value of k. If that is done by beginning with what is essentially a Bickley sinuous mode at moderate k, we obtain the results shown in figures 4 and 5. However, for proceeding toward smaller and smaller values of k, a beginning made with a Bickley varicose mode at moderate k gives the results shown in figures 8 and 9, which disagree with the theory. A detailed investigation of the eigenfunctions during this k-decreasing iteration shows that the eigenfunction changes character at longer wavelengths – the mode ceases to be obviously 'varicose'. It appears that the numerical k-marching procedure goes onto a sinuous branch of the solution, rather than remaining 'varicose'. Again, we note that the 'sinuous' and 'varicose' modes of §§4 and 5 are in fact long-wave analytic continuations of sinuous and varicose Bickley modes, since those words become meaningless once the eigenfunction grows to include the regions outside the jet, *per se*. We remain convinced of the validity of the varicose-mode asymptotics *in spite of* the lack of numerical corroboration.

We note here that, theoretically, the higher modes of the varicose family probably emerge from the infinitely many branches of the inverse-tangent function arising in the internal layer III of §5, when applied to higher-order matching, although this does not seem to affect the comparisons above. In addition, the existence of another family of varicose modes different from those of the present study cannot be discounted yet.

Next, the contrast between the sinuous modes of §4 and the varicose ones of §5 is of interest. Although the structures and the strong interactions between the various zones are rather involved the separate physical features of the sinuous and the varicose modes are fairly clear for most axial wavenumbers k. The sinuous disturbances are driven by the pressure jump across the axial ring jet due to the coanda effect in the sinuous motion, whereas for the varicose disturbances the jump across the jet is in the pressure gradient as opposed to the pressure itself and, correspondingly, the critical layer embedded in the jet plays a vital role in ensuring that the jump properties hold. This distinction continues to hold until, in the varicose case, the regimes (*b*), (*c*) are encountered at low k, bringing in three-dimensional and basic-swirl centrifugal effects, in addition, which serve to gradually alter the jump conditions across the ring jet. A similar phenomenon occurs for the sinuous case at reduced wavenumbers and also at larger k-values. Further, the present alternative approach to the stability problem demonstrates that the interactive nature of the fully three-dimensional solutions is rich in interest, with emphasis on the delicate physical balances involved and the finding of unstable solutions for all positive and negative (and zero) azimuthal wavenumbers n, in contrast with many previous studies of swirling-flow stability.

The same approach may well be useful in increasing the understanding of the Type I Long's vortex stability and for other swirling flows such as the trailing vortex and rotating pipe flow. It is believed that certain viscous and non-parallel-flow effects, which could subsequently affect the longer waves at small k, can also be incorporated.

The influence of nonlinearity would seem to be the most crucial area of further research, however, as emphasized in §1, and here the flow structures laid out in §§4 and 5 appear to provide a good starting point. Nonlinear effects are likely to come into force either through significant movement of the axial ring jet itself, akin to a vortex sheet, or through a nonlinear critical-layer process since a kind of linear critical layer acts in the case of the varicose modes of §5. It remains to be seen, from

the present and other theories, whether a closer connection with the real phenomenon of vortex breakdown can be established or not by inclusion of nonlinear effects. Again, another promising different view of the breakdown may emerge from steady-flow theory as in Burggraf & Foster's (1977*b*) marching computations of the boundary-layer equations, which in some cases lead to a singularity within a finite distance. That may herald the onset of a large-scale separated eddy or vortex, with swirl, and this also remains to be investigated.

Another alternative, for tackling nonlinearity in rotating pipe flow, is to consider the consequences of added swirl in the Smith & Bodonyi (1982) finding of nonlinear neutral modes in Hagen–Poiseuille flow.

The computations were performed on the IBM 3081 of the Instruction and Research Computer Center of The Ohio State University and the CRAY XMP1 of the NASA Lewis Research Center. The work herein was carried out in part under support for M. R. F. from SERC in the form of a Visiting Professor Fellowship in the summer of 1985, and also from NASA Lewis ICOMP, during the summer of 1987.

Appendix

Equations (2.2) may be combined into a single secord-order equation which may be simplified somewhat (cf. Leibovich & Stewartson 1983) for our purposes here to represent the eigenfunction on the jet region of the vortex,

$$\frac{\mathrm{d}^2u}{\mathrm{d}\xi^2} = k^2Ku, \quad K = 1+\frac{a}{\phi}+\frac{b}{\phi^2}, \tag{A 1a,b}$$

$$A = k^{-1}(\mathscr{W}'+\frac{n}{y_0^2k^2}\mathscr{G}')', \quad b = -\frac{2\mathscr{G}}{ky_0^3}(k\mathscr{G}'-n\mathscr{W}'), \tag{A 1c,d}$$

$$\phi = k(\mathscr{W}-c)+n\mathscr{G}/y_0^2. \tag{A 1e}$$

As mentioned briefly in §6, the arguments leading to the upper cut-off, k_c, for the Bickley jet (see Drazin & Reid 1981, for example) cannot be applied here since the angular momentum of the vortex becomes important, just as at small k. For the upper cut-off, it appears that the proper scalings are

$$c = \mathscr{W}(0)+\frac{n}{y_0^2k}\mathscr{G}(0)+\tfrac{1}{2}\mathscr{W}''(0)\,\alpha^2y_0^{-3}c_1+\ldots,$$

where $k = y_0^{\frac{3}{2}}\alpha$ and $a_2\,(\xi+\sqrt{2}) = y_0^{-\frac{3}{2}}\sqrt{2}x$. Recall that $\mathscr{W}'(0) = 0$. Substituting these into (A 1), along with similar Taylor series expansions for (a, b), leads to the following equation:

$$\frac{\mathrm{d}^2u}{\mathrm{d}\xi^2} = 16\left[\alpha^2+\frac{1}{x^2-c_1}-\frac{p}{(x^2-c_1)^2}\right]u, \tag{A 2}$$

where $p = 128/\sqrt{2}$. Multiplying (A 2) by $\bar{u}$, and integrating across the vortex leads to the solvability condition

$$c_{1\mathrm{I}}\int_{-\infty}^{\infty}|u|^2\left(\frac{1}{|x^2-c_1|^2}+2p\frac{c_{1\mathrm{R}}-x^2}{|x^2-c_1|^4}\right)\mathrm{d}x = 0$$

From which it is quite clear that solutions for $c_{1\mathrm{I}} > 0$ may indeed exist.

As $k \to k_c$ (or, here, $\alpha \to \alpha_c$), $c_{1I} \to 0$, and apparently also $c_{1R} \to 0$. In such a case, the equation for the neutral eigenfunction is

$$\frac{d^2u}{dx^2} = 16\left[\alpha c^2 + \frac{1}{x^2} - \frac{p}{x^4}\right]. \tag{A 3}$$

WKBJ methods show that, for $x \to 0$, the two approximate solutions of (A 3) are

$$\sin(4p^{\frac{1}{2}}/x), \quad \cos(4p^{\frac{1}{2}}/x),$$

one corresponding to a sinuous eigenfunction (the cosine), and one to the varicose mode (the sine). At large $|x|$, clearly the decay is exponential, as $\exp(\pm\alpha_c x)$.

To explore solutions to (A 3), we write

$$\alpha c^{\frac{1}{2}} x = p^{\frac{1}{4}} \exp(\mathrm{i}(v + \tfrac{1}{4}\pi)), \tag{A 4}$$

whose substitution into (A 3) gives the Mathieu equation for $P = u/x^{\frac{1}{2}}$,

$$(d^2P/dv^2) + [a - 2q\cos(2v)]P = 0, \tag{A 5}$$

where $a = \frac{65}{4}$ and $q = -\mathrm{i}\alpha_c p^{\frac{1}{2}}$. We note from (A 4) that at $x = -\infty$, $v = -\mathrm{i}\infty + \pi$; at $x = 0$, $v = \mathrm{i}\infty + \frac{1}{2}\pi$; and at $x = \infty$, $v = -\mathrm{i}\infty + 0+$; so v is a complex variable. From Abramowitz & Stegun (1965), we consider a solution of (A 5),

$$P_1 = Ce_R(\mathrm{i}v) = Ce_R(-\tfrac{1}{4} + \mathrm{i}\log(\alpha_c^{\frac{1}{2}} x/p^{\frac{1}{4}})), \tag{A 6}$$

where the notation is for the Rth even periodic solution of (A 5). In general, such solutions of (A 5) exist for particular values of $a_r(q)$. Apart from certain multiplicative constants, $Ce_R(z)$ has the following asymptotic behaviour,

$$Ce_R(z) \sim \frac{\cos(2q^{\frac{1}{2}}\cosh(z) - \frac{1}{2}r\pi - \frac{1}{4}\pi)}{p^{\frac{1}{2}} q^{\frac{1}{4}} [\cosh(z) - \sigma]^{\frac{1}{2}}}, \quad |z| \to \infty, \tag{A 7}$$

where σ is arbitrary. Application of (A 7) for $x \to 0$ under (A 6) shows that this solution behaves like $\cos(4p^{\frac{1}{2}}/x)$ near $x = 0$, meaning that this is clearly a sinuous eigenfunction. For $|x| \to \infty$, application of (A 7) shows that the behaviour is

$$P_1 \sim \exp(-\tfrac{1}{8}\mathrm{i}\pi)\left[\frac{p^{\frac{1}{4}}}{\alpha c^{\frac{1}{2}}}\right]\frac{\cosh(\alpha_c x)}{x^{\frac{1}{2}}}, \tag{A 8}$$

which does not decay for $x \to \infty$, since $u = x^{\frac{1}{2}}P$. Now, Mulholland & Goldstein (1929) have found that (A 5) has solutions for pure imaginary q. In particular, they found that a_0 and a_2 (corresponding to Ce_0 and Ce_2) have identical values at $q = -1.469\,\mathrm{i}$. Thus, since the form of (A 8) is r-independent, both Ce_0 and Ce_2 have *identical* asymptotic forms. Hence, the solution

$$u = x^{\frac{1}{2}}[Ce_0(-\tfrac{1}{4}\mathrm{i}\pi + \log(\alpha_c^{\frac{1}{2}} x/p^{\frac{1}{4}})) - Ce_2(-\tfrac{1}{4}\mathrm{i}\pi + \log(\alpha_c^{\frac{1}{2}} x/p^{\frac{1}{4}}))] \tag{A 9}$$

will decay for $|x| \to \infty$, and its eigenvalue q is $-1.469\mathrm{i}$. Hence,

$$\alpha_c = 1.469/p^{\frac{1}{2}}. \tag{A 10}$$

Therefore, $k_c = 1.469\, y_0^{\frac{3}{2}}/(128/\sqrt{2})^{\frac{1}{2}}$. For the case run here ($M = 44.9$), this computed k_c-value is 72.91.

So, the presence of swirl in the sinuous mode greatly extends the range of unstable wavenumbers over the Bickley-jet case. The above analysis does not appear to go through for the varicose case; no comparable eigensolutions for pure imaginary q of the Co_R variety (odd symmetry) are known to us in the literature.

REFERENCES

ABRAMOWITZ, M. & STEGUN, I. A. 1965 *Handbook of Mathematical Functions*. Dover.

BATCHELOR, G. 1964 Axial flow in trailing line vortices. *J. Fluid Mech.* **20**, 645.

BURGGRAF, O. R. & FOSTER, M. R. 1977*a* The stability of tornado-like vortices. *Final Rep.*, Grant No. 04-6-022-44004. US Department of Commerce.

BURGGRAF, O. R. & FOSTER, M. R. 1977*b* Continuation or breakdown in tornado-like vortices. *J. Fluid Mech.* **80**, 685.

CHURCH, C. R. & EHRESMAN, C. M. 1971 A brief report on the Purdue waterspout research program. *Purdue Tornado Project Rep.*

DRAZIN, P. G. & HOWARD, L. N. 1966 Hydrodynamic stability of parallel flow of inviscid fluids. *Adv. Appl. Math.* **7**, 1.

DRAZIN P. G. & REID, W. H. 1981 *Hydrodynamic Stability*. Cambridge University Press.

DUCK, P. W. 1986 The inviscid stability of swirling flows: large wavenumber disturbances. *Z. Angew. Math. Phys.* **37**, 340.

DUCK, P. W. & FOSTER, M. R. 1980 The inviscid stability of a trailing line vortex. *Z. Angew. Math. Phys.* **31**, 524.

FOSTER, M. R. & DUCK, P. W. 1982 Inviscid stability of Long's vortex. *Phys. Fluids* **25**, 1715.

GOLDEN, J. H. 1973 Life cycle of the Florida Keys waterspout as a result of five interacting scales of motion. Ph.D. thesis, Florida State University, Tallahassee.

HOECKER, W. H. 1960 Windspeed and air flow patterns in the Dallas tornado of April 7, 1957. *Mon. Weather Rev.* **88**, 167.

HOWARD, L. N. & GUPTA, A. S. 1962 On the hydrodynamic and hydromagnetic stability of swirling flows. *J. Fluid Mech.* **14**, 473.

LEIBOVICH, S. & STEWARTSON, K. 1983 A sufficient condition for instability of columnar vortices. *J. Fluid Mech.* **126**, 335.

LESSEN, M., DESPHANDE, N. V. & HADJI-OHANES, B. 1973 Stability of a potential vortex with a non-rotating and rigid-body rotating top-hat jet core. *J. Fluid. Mech.* **60**, 459.

LESSEN, M. & SINGH, P. J. 1973 The stability of axisymmetric free shear layers. *J. Fluid Mech.* **60**, 433.

LESSEN, M., SINGH, P. J. & PAILLET, F. 1974 The stability of a trailing line vortex. *J. Fluid Mech.* **63**, 753.

LONG, R. R. 1961 A vortex in an infinite fluid. *J. Fluid. Mech.* **11**, 611.

MASLOWE, S. & STEWARTSON, K. 1982 On the linear inviscid stability of rotating Poiseuille flow. *Phys. Fluids* **25**, 1517.

MULHOLLAND, H. P. & GOLDSTEIN, S. 1929 The characteristic numbers of the Mathieu equation with purely imaginary parameters. *Phil. Mag.* **8**, 834.

PEDLEY, T. 1968 On the instability of rapidly rotating shear flows to non-axisymmetric disturbances. *J. Fluid Mech.* **31**, 603.

PEDLEY, T. 1969 On the instability of viscous flow in a rapidly rotating pipe. *J. Fluid Mech.* **35**, 97.

SMITH, F. T. & BODONYI, R. J. 1982 Non-linear critical layers and their development in streaming-flow stability. *J. Fluid Mech.* **118**, 165.

SNOW, J. T. 1978 On inertial instability as related to the multiple vortex phenomenon. *J. Atmos. Sci.* **35**, 1660.

SQUIRE, H. 1951 The round laminar jet. *Q. J. Mech. Appl. Maths* **4**, 321.

STALEY, D. O. & GALL, B. L. 1979 Barotropic instability in a tornado vortex. *J. Atmos. Sci.* **36**, 973.

STEWARTSON, K. 1982 The stability of swirling flow at large Reynolds number when subjected to disturbances with large azimuthal wavenumber. *Phys. Fluids* **25**, 1953.

STEWARTSON, K. & CAPELL, K. 1985 Marginally stable ring modes in a trailing line vortex: upper neutral point. *J. Fluid Mech.* **156**, 369.

STEWARTSON, K. & LEIBOVICH, S. 1987 On the stability of a columnar vortex to disturbances with large azimuthal wavenumber: the lower neutral points. *J. Fluid Mech.* **178**, 549.